Angewandte Chemie
Eine Zeitschrift der Gesellschaft Deutscher Chemiker

Supporting Information

Vacancy-Enabled O3 Phase Stabilization for Manganese-Rich Layered Sodium Cathodes

Biwei Xiao[+], Yichao Wang[+], Sha Tan[+], Miao Song, Xiang Li, Yuxin Zhang, Feng Lin, Kee Sung Han, Fredrick Omenya, Khalil Amine, Xiao-Qing Yang, David Reed, Yanyan Hu, Gui-Liang Xu, Enyuan Hu,* Xin Li,* and Xiaolin Li**

anie_202016334_sm_miscellaneous_information.pdf

Experimental

Material synthesis

The precursor $Mn_{0.68}Ni_{0.16}Co_{0.16}(OH)_2$ was synthesized via a co-precipitation method. Stoichiometric amount of $MnSO_4 \cdot H_2O$ (Aldrich, 99%), $NiSO_4 \cdot 6H_2O$ (Aldrich, 99%) and $CoSO_4 \cdot 7H_2O$ (Aldrich, 99%) were mixed to form solution A with a total concentration of 1 M. NaOH (2M) and ammonia (0.15M) were mixed to form solution B. Solutions A and B were subsequently pumped into the reactor by peristatic pumps separately at a speed of 1mL/min under an agitation speed of 400 rpm, the reactor temperature was controlled to be 60 ^oC, and the PH was set to be 11.2. After reacting for 10 h, the precipitate was harvested and thoroughly washed with de-ionized water and dried in vacuum. Afterwards, the hydroxide precursor was mixed with stoichiometric amount of Li_2CO_3 (Aldrich, 99%) thoroughly and sintered under 500 ^oC for 5 h and 900 ^oC for 12 h to obtain the final LRNMC material $Li_{1.2}Mn_{0.54}Ni_{0.13}Co_{0.13}O_2$.

Characterization

Electrochemical measurements: The LRNMC electrodes were prepared by casting the mixture of LRNMC powder, super P and polyvinylidene fluoride (PVDF) in N-metrhyl-2pyrrolidone (NMP) with a mass ratio of 80:10:10 on Al foil and dried at 120 ^oC in a vacuum oven. The electrodes were tested in CR2032 coin cells using either Li or Na metals as the counter electrode. To de-lithiate the LRNMC, the electrode was assembled into a coin cell using Celgard polyethylene separator, 1M $LiPF_6$ dissolved in ethylene carbonate (EC) and dimethyl carbonate (DMC) (1:1 wt%) electrolyte and Li as the counter electrode. The cell was thereafter charged to 4.6 V and disassembled to harvest the de-lithiated electrode. Then, the de-lithiated electrode was assembled into a coin cell using Na metal as the counter electrode, and 1M $NaPF_6$ (Kishida, Japan) dissolved in tetraglyme (TEGDME, Oakland Chemicals). The active material loading in the electrode is ~ 4 mg/cm^2. The cell was then discharged to 2 V and charged to 3.8 V followed by continuous cycling. For the NMC333 control study, the cell was de-lithiated to 4.5 V vs Li/Li^+, followed by the same test in Na electrolyte against Na metal. Galvanostatic intermittent titration (GITT) was carried out to determine the Na-ion diffusion rate (D_{Na+}) using the same cell configurations, the testing protocol is composed of 10 min galvanostatic pulse at 12.5 mA/g and 120 min of relaxation time.

Transmission electron microscopy (TEM) Characterization: TEM specimens are prepared using a focused ion beam (FEI Helios NanoLab 600i). For the FIB samples, 1.2 μm thick Pt layer (200 nm e-beam deposition followed by 1 μm ion beam deposition) was deposited first on the particles to avoid Ga ion beam damage. Then the specimens were thinned to 200 nm using 30 kV Ga ion beam. A final polishing was performed using 2 kV Ga ion beam to remove the surface damage layer and further thinning to electron transparency. Scanning transmission electron microscopy (STEM) was carried out on a FEI Titan G2 60-

300 microscope with a probe spherical aberration corrector, enabling sub-angstrom imaging using high-angle annular dark-field scanning transmission electron microscopy (STEM-HAADF) detectors at 300 kV. For STEM-HAADF imaging, the inner and outer collection angles of an annular dark-field detector were 58.5 and 200 mrad, respectively.

In-situ X-ray diffraction (XRD): In situ XRD of the sodiation/desodiation processes of the de-lithiated LRNMC4.6 cathodes during charge/discharge were measured at Beamline 11-ID-C of Advanced Photon Source at Argonne National Laboratory. The wavelength is 0.117418 (± 0.15%) Å. Coin cells with holes for beam pass were used to make the in-situ cell. The holes at the top and bottom cases of the coin-cell were sealed with Kapton tape after cell assembly. The electrode had a mass loading of ≈5 mg/cm^2, the in-situ cell was rested for 5 h before doing in-situ XRD. During the in-situ experiment, an MACCOR cycler was used to discharge/charge the cell using a constant rate of 10 mA/g between 2.0 and 3.8 V.

Ex situ XRD/pair distribution function (PDF) analysis: X-ray diffraction experiments were carried out using beamline 28-ID-2 (λ = 0.1971(1) Å) at National Synchrotron Light Source II of Brookhaven National Laboratory. The ex situ samples were collected from disassembling the cell at desired stage and washing the electrodes in dimethyl carbonate (DMC) followed by grinding into fine powders. Powders were then packed into a 1.2 mm diameter capillary and sealed by epoxy in the Argonne-filled glove box. Capillaries are then measured at the beamline in transmission mode by placing an amorphous silicon area detector (Perkin-Elmer) around 1360 mm from the sample. Raw image data was integrated using the program Fit2D[1]. Le Bail fitting or Rietveld refinement was carried out using TOPAS[2]. X-ray pair distribution function (PDF) experiments were carried out at beamline 28-ID-2 at National Synchrotron Light Source II of Brookhaven National Laboratory using an X-ray energy of 66.7 keV (λ = 0.1971(1) Å) and an amorphous silicon area detector (Perkin-Elmer) close to the sample-containing capillaries (around 200 mm) to obtain data to large momentum transfer values. Data were integrated using the program Fit2D. PDFgetX3[3] used to correct the data for background contributions, Compton scattering and detector effects, and to Fourier transform (Q_{max} = 23 Å^{-1}) the data to generate G(r), the PDF.

Synchrotron XAS studies: The transition metal K-edge XAS spectra including X-ray absorption near edge structure (XANES) and extended X-ray absorption fine structure (EXAFS) were measured at 7-BM beamline of National Synchrotron Light Source II (NSLS II), Brookhaven National Laboratory (BNL). During data acquisition, reference spectra of metal foils were collected simultaneously for energy calibration. As-obtained XAS spectra were analyzed using the Athena package. The EXAFS data was Fourier transformed to R-space data, which is fitted against the layered structure model using Artemis software to obtain local structure information including bond length, coordination number. The coordination number of Ni and Co is fixed and that of Mn is fitted using the model.

Nuclear magnetic resonance (NMR) measurement: ^{7}Li MAS NMR experiments were performed on a Bruker Advance III spectrometer in a 14.1 T magnetic field with a 7Li Larmor frequency of 233.21 MHz. Electrodes were packed into 1.3 mm rotors and spun at a MAS rate of 50 kHz.

Computational methods

DFT: All DFT calculations in this work were performed using the Vienna Ab initio Simulation Package within the projector augmentedwave approach using the Perdew–Burke–Ernzerhof GGA functional and the GGA+U extension to it. The U values for Mn, Co, and Ni were 3.9, 3.4, and 6.0 eV, respectively, in line with previous literature.[4] $Na_8Mn_9Ni_2Co_2\square_3O_{32}$ supercells with size 4 × 4 × 1 (2 × 2 × 2 Gamma centered k-point) were used. A 520 eV plane-wave energy cutoff was used for all calculations. The Van der Waals interaction was treated by DFT-D3BJ method.[5] The TM ordering before considering TM migration was manually created to allow TM mixing and was fixed for all structures. 2 TM migrations per supercells were considered, and each of them had separate TM vacancy as neighbor. Na orderings were the low energy orderings at 50% sodium composition when there were no migration in O3 or P3 structure[6], or with modification to allow/forbid small distance (< 2 Å) between sodium ions and migrated TMs in the initial structure before the relaxation. The structures were fully relaxed.

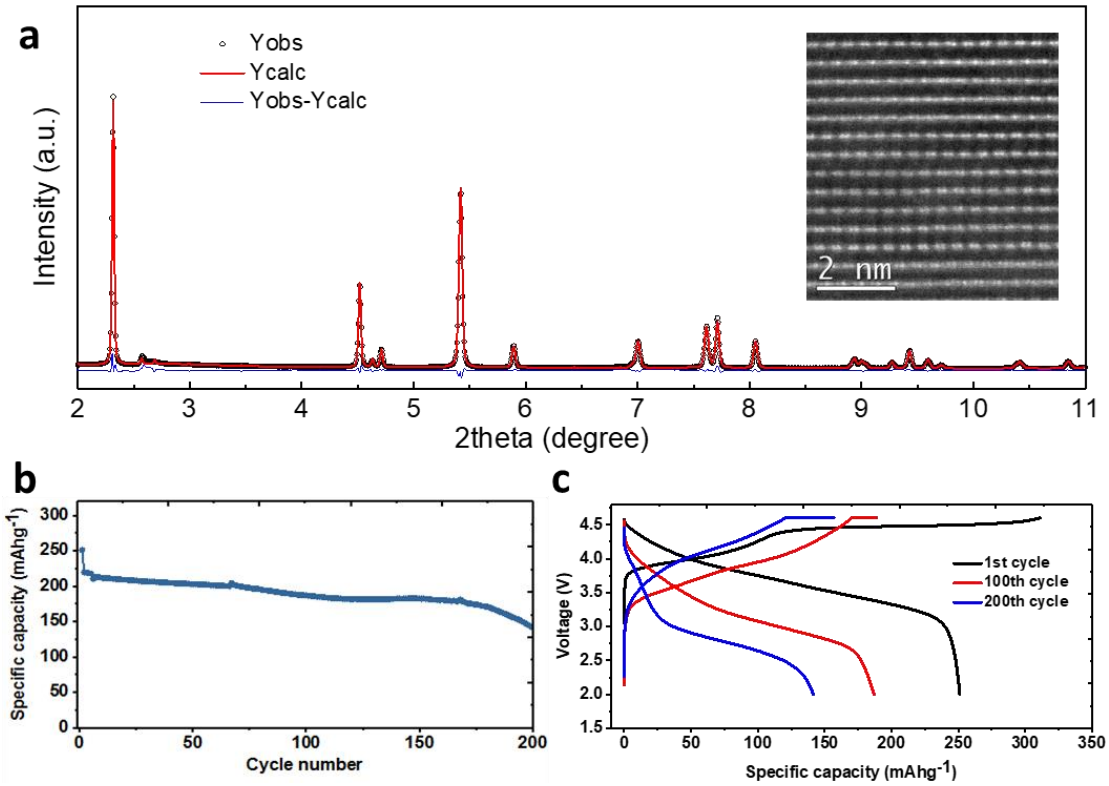

Figure S1 (a) Rietveld refinement of the pristine LRNMC (inset: HAADF-STEM image showing the TM-TM dumbbell structure) (b-c) Electrochemical performance of the LRNMC tested at 125 mA/g, first cycle was tested under 12.5 mA/g)

In refining the pristine structure of LRNMC, cation mixing was considered for a good fitting. Specifically, Mn and Co are allowed to occupy 2b site which was originally dominated by Li and Ni; Li and Ni are allowed to occupy 4g site which was originally dominated by Mn and Co. Considering that Ni^{2+} and Li^{+} have similar cation size, the possibility of Ni entering the lithium-dominated layer is also considered. More complicated mixing may be unlikely and usually are not considered in the literature.[7] Initial fitting led to negative thermal displacement parameters (B values) for those lithium-dominant sites. To fix this, B values of lithium-dominant sites are fixed to those reported in the literature that uses neutron diffraction data.[7a]

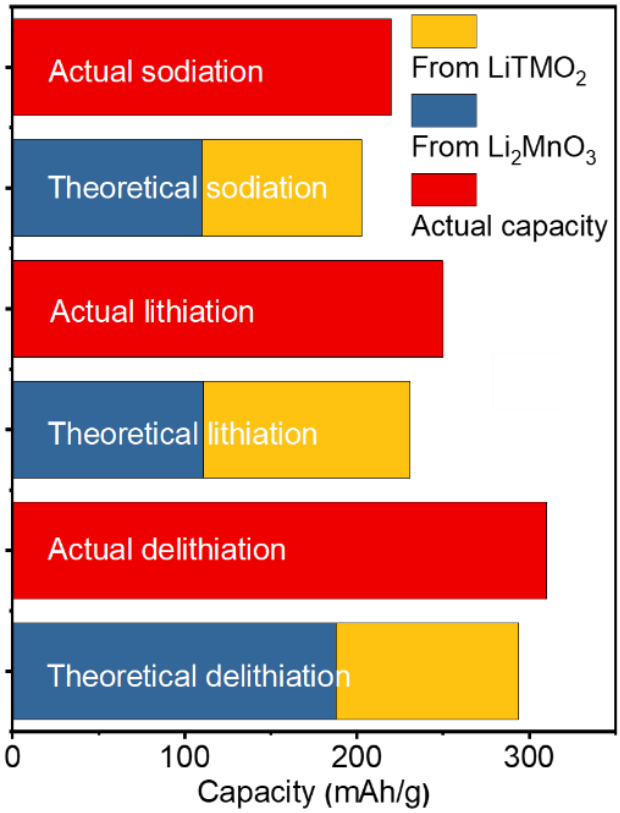

Figure S2. Bar chart showing the experimental and theoretical capacities of LRNMC at 4.6V de-lithiation, 2V lithiation and 2V sodiation (the theoretical capacities were calculated based on the contributions from Li_2MnO_3 and $LiTMO_2$ in $xLi_2MnO_3 \cdot (1-x)LiTMO_2$ respectively).

The theoretical and experimental capacity contribution was calculated based on LRNMC $Li_{1.2}[Mn_{0.66}Co_{0.17}Ni_{0.17}]_{0.8}O_2$, which can be rewritten into the combination of $0.41[Li_2MnO_3] \cdot 0.39[Li(Mn_{0.33}Co_{0.33}Ni_{0.33})O_2]$. The theoretical charge capacity of Li_2MnO_3 is 458 mAh/g assuming the activation of it into Li^+, MnO_2 and O_2, while the theoretical charge capacity of $Li(Mn_{0.33}Co_{0.33}Ni_{0.33})O_2$ is 271 mAh/g. Theoretical lithiation and sodiation capacities are estimated by assuming the intercalation of Li or Na into MnO_2 and $(Mn_{0.33}Co_{0.33}Ni_{0.33})O_2$ units. LRNMC has a theoretical lithiation capacity of 231 mAh/g while the NaLRNMC theoretical sodiation capacity is 202 mAh/g. The actual de-lithiation capacity is very close to the theoretical value and the slightly higher value (16 mAh/g) is supposed to arise from the electrolyte decomposition. Actual lithiation capacity is 18 mAh/g lower than the theoretical capacity, presumably due to the reduction of oxygen.[8] The actual sodiation capacity is ~220 mAh/g, which is also 18 mAh/g higher than the theoretical sodiation capacity.

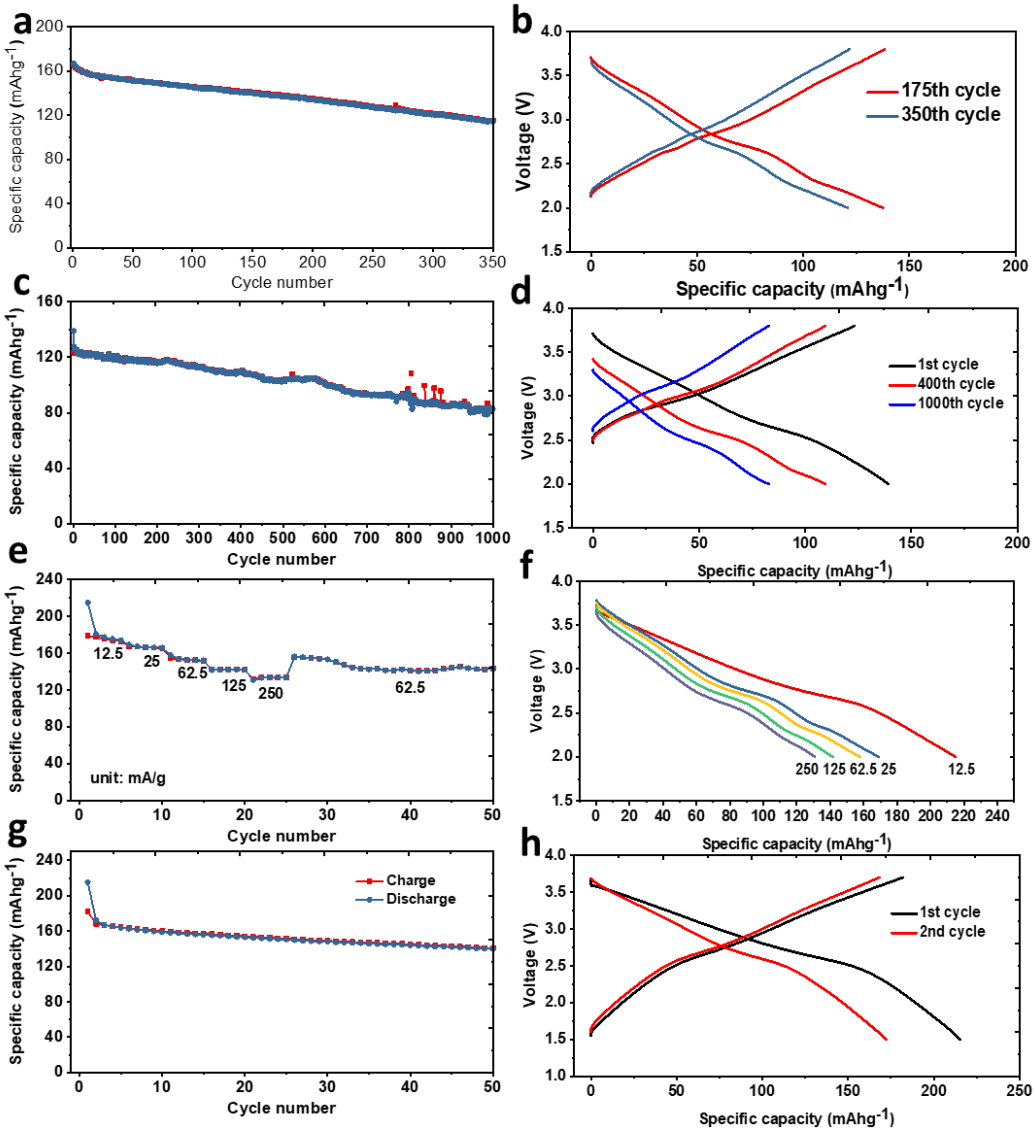

Figure S3 (a-b) Performance at 62.5 mA/g. (c-d) Performance at 250 mA/g. (e-f) Rate capability. (g-h) Full cell performance paired with hard carbon at 62.5 mA/g

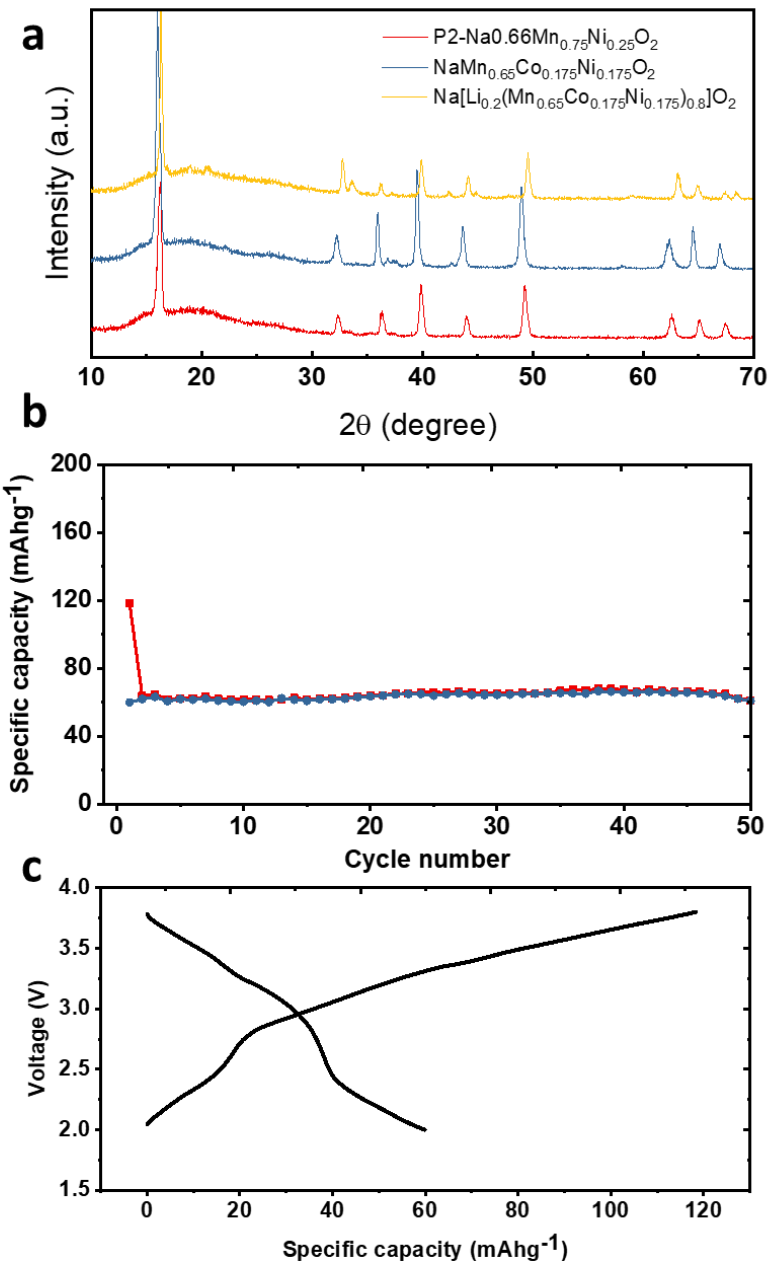

Figure S4 (a) XRD patterns of $Na(Mn_{0.66}Co_{0.17}Ni_{0.17})O_2$ and $Na[Li_{0.2}(Mn_{0.66}Co_{0.17}Ni_{0.17})_{0.8}]O_2$. (b-c) Performance of $Na(Mn_{0.66}Co_{0.17}Ni_{0.17})O_2$

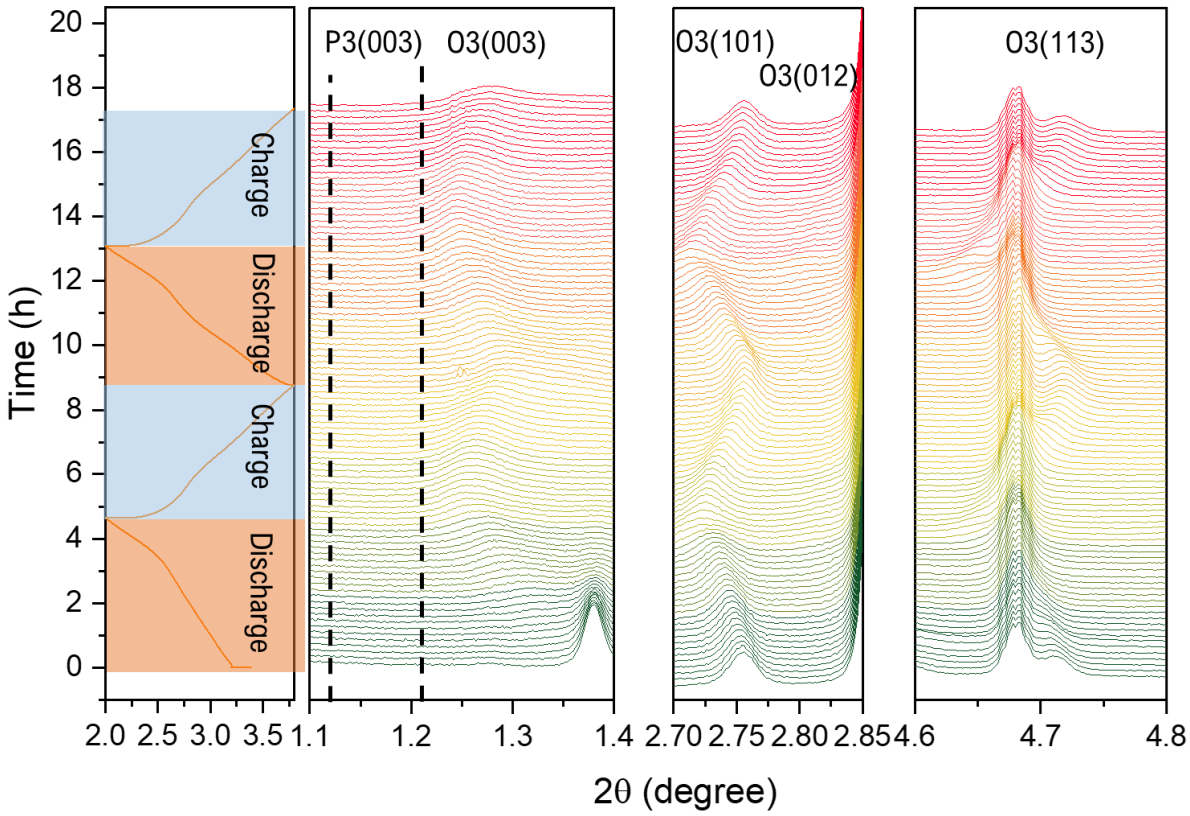

Figure S5 Line plot of the in-situ XRD in Figure 1

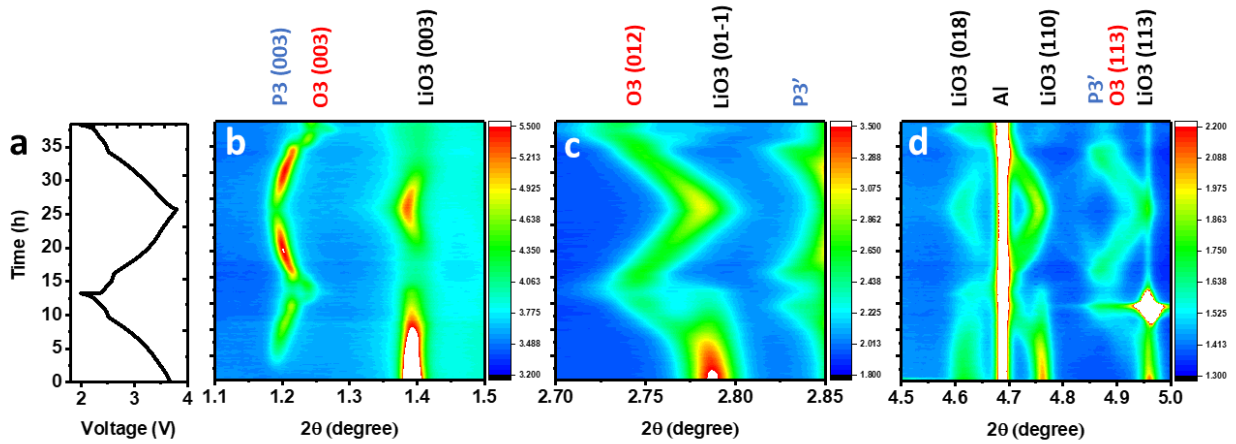

Figure S6 In-situ XRD of the sodiation/de-sodiation processes of regular layered $LiNi_{1/3}Co_{1/3}Mn_{1/3}O_2$ (NMC333) de-lithiated to 4.5 V (vs Li/Li^+).

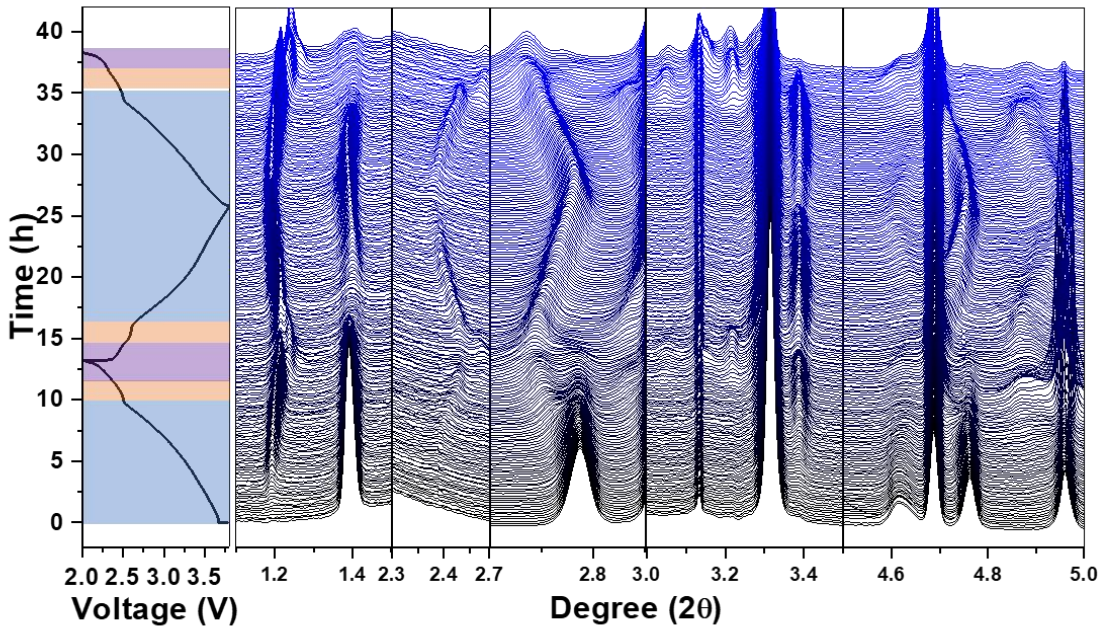

Figure S7 Line plot of in-situ XRD of the sodiation/de-sodiation processes of regular layered $LiNi_{1/3}Co_{1/3}Mn_{1/3}O_2$ (NMC333) de-lithiated to 4.5 V (vs Li/Li^+).

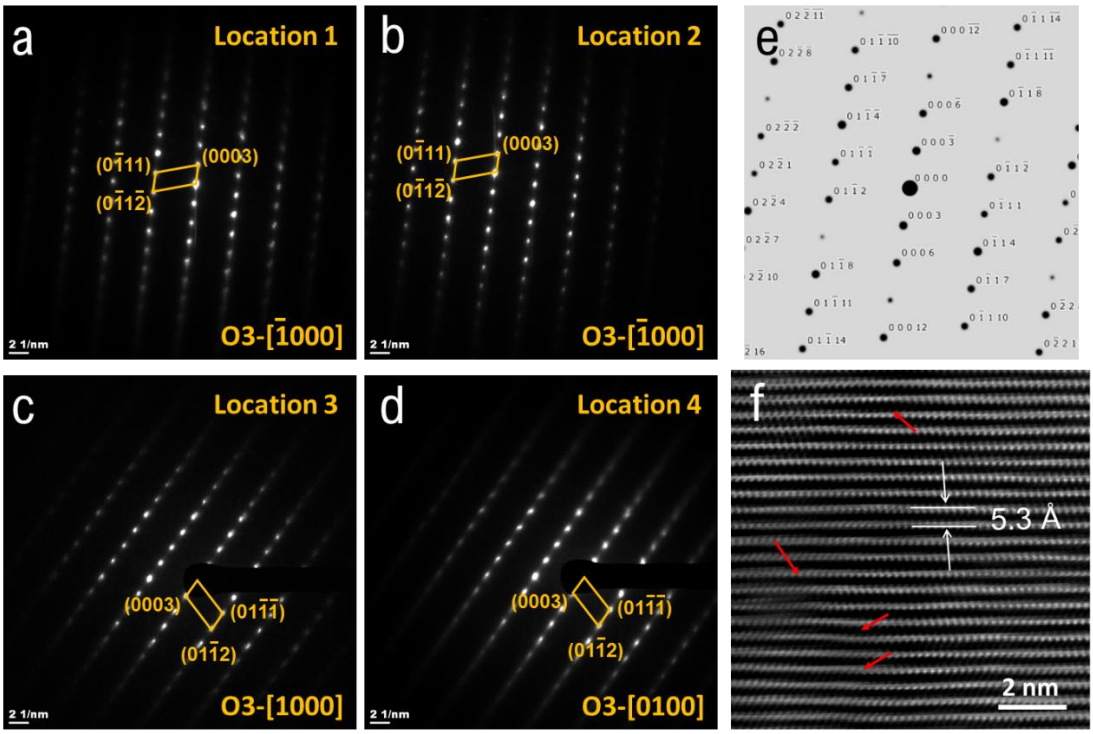

Figure S8. (a-d) Selected area electron diffraction (SAED) patterns of random NaLRNMC particles charged to 3V. (e) standard diffraction pattern of O3 structured layer material. (f) Typical HAADF image of a NaLRNMC particle charged to 3V. Red arrows show the distorted layers.

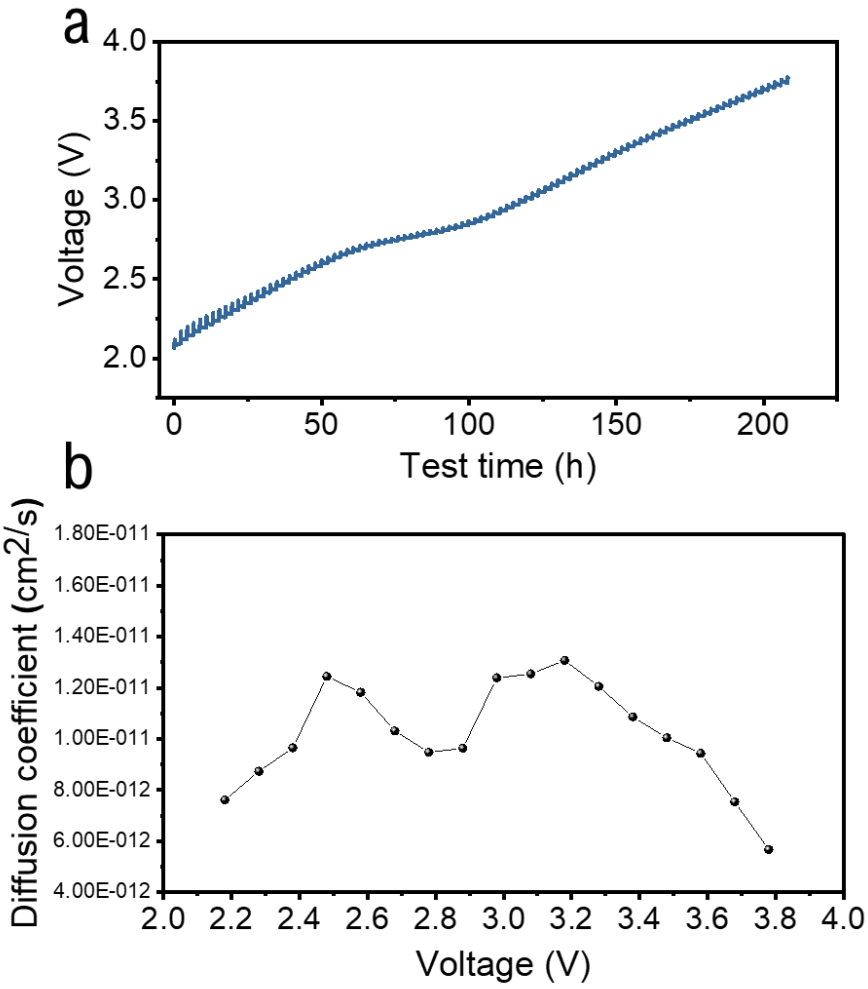

Figure S9 (a) GITT plots of NaLRNMC during the charging process. (b) Calculated Na-ion diffusion coefficient.

The Na-ion diffusion coefficient (D_s) was determined by GITT following the GITT diffusivity formula below:

$$D_S = \frac{4}{\pi\tau}\left(\frac{R_S}{3}\right)^2\left(\frac{\Delta E_S}{\Delta E_t}\right)^2$$

Where τ is the time duration of the pulse, R_s is the radius of the spherical particle (1 μm), ΔE_s is the steady-state voltage change and ΔE_t is the voltage change during the constant current pulse.[9]

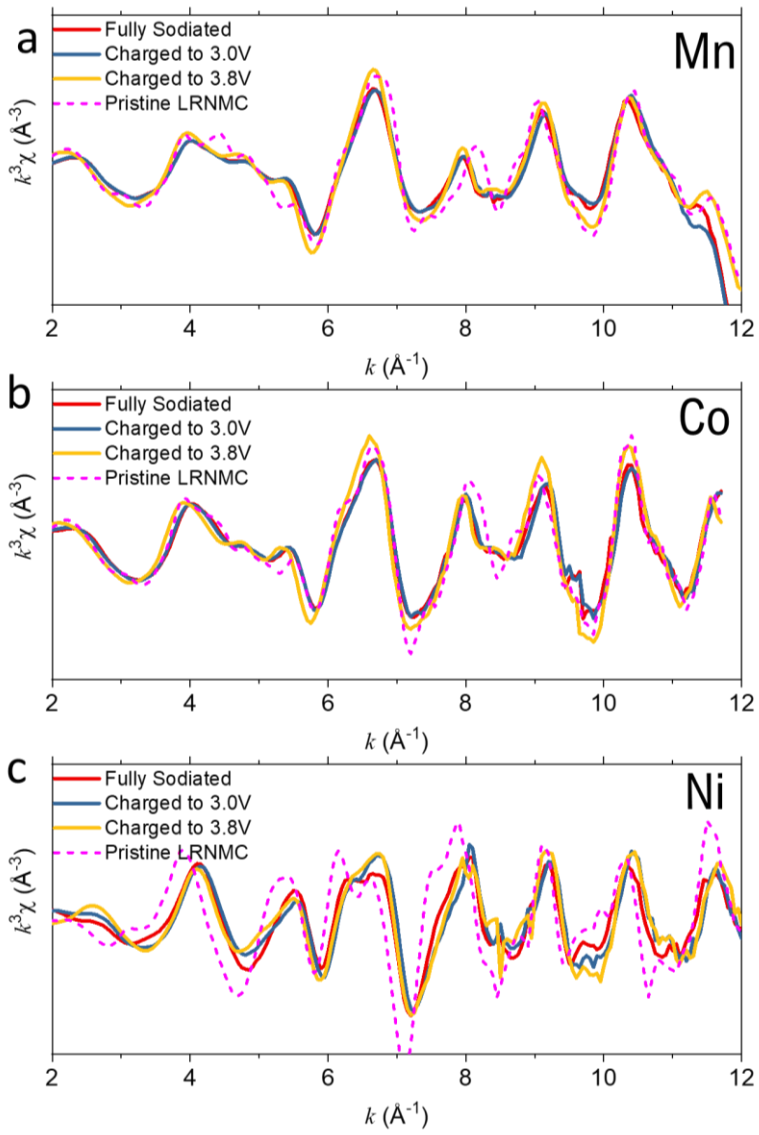

Figure S10. *k*3 weighted EXAFS data of Ni, Mn, and Co for ex situ samples.

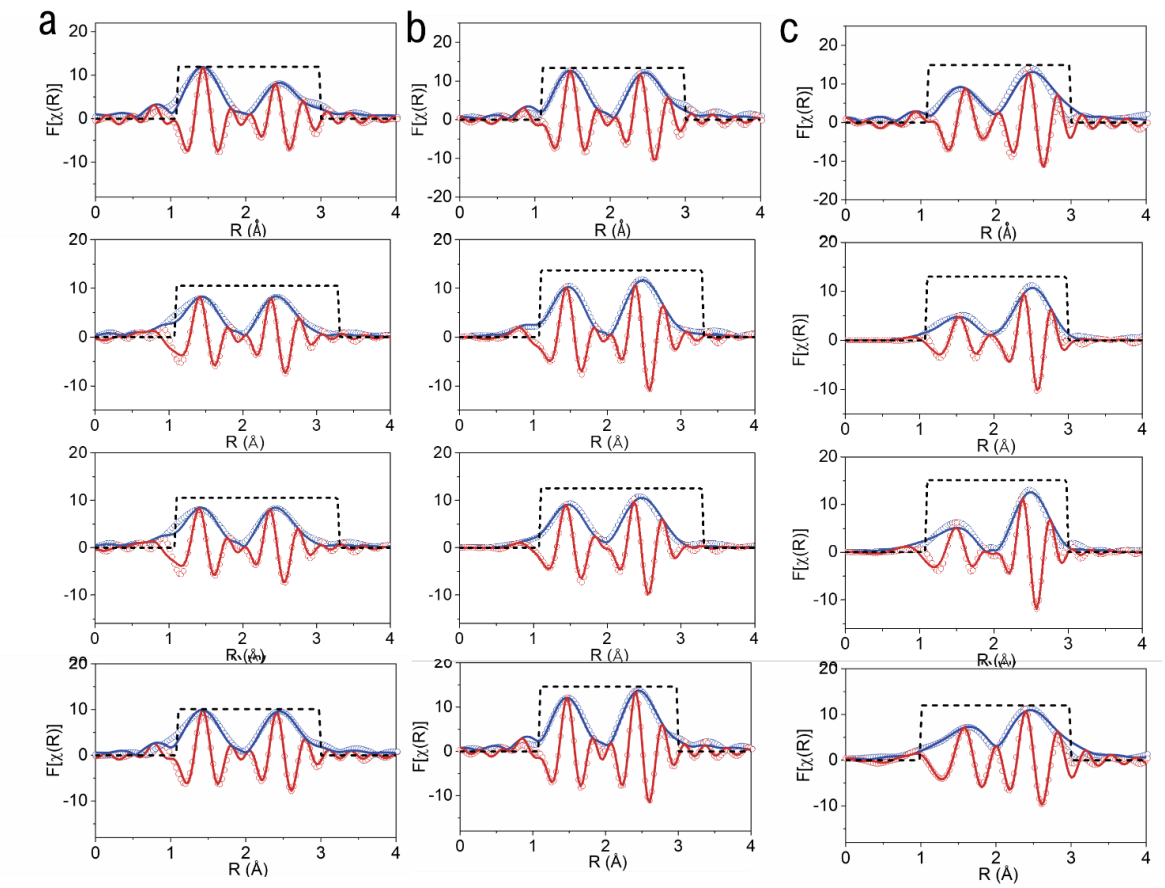

Figure S11. Fitted ft-EXAFS data of (a) Mn, (b) Co, and (c) Ni. In all cases, the upper panel corresponds to the pristine LRNMC, the 2nd panel, fully sodiated sample; the 3rd panel, charged to 3V sample; the lower panel, charged to 3.8V sample. The dash line corresponds to the fitting range in R space.

Extended X-ray absorption fine structure (EXAFS) arises from the interaction between outgoing photoelectron and neighboring atoms. After Fourier transform (ft), it can directly reveal the local structural information. Figure S10 indicates that high quality *k* space data can be obtained (up to 11 $Å^{-1}$) which enables a reliable Fourier transform and high quality *R* space data. The ft-EXAFS for Mn, Co, and Ni in the ex-situ samples are presented in Figure 2f-h. In fitting the ft-EXAFS data, a layered structure model that has TM-O as the first shell and TM-TM as the second shell is used. Figure S11 shows that excellent fitting is achieved for all the ex-situ samples. It is worth noting that because Debye-Waller factor and coordination number are highly correlated, it is difficult to separate their contributions to the ft-EXAFS and fit them freely. After several trials, it was found out that fitting all the coordination numbers freely would lead to either unstable fitting or unreasonable results. Finally, a fitting strategy that fixes the first shell coordination number and only varies the second shell coordination number for Mn is used. Detailed fitting results are summarized in Table S3-5.

Table S1 Rietveld refinement results of the pristine LRNMC

Space group: *C*2/m a=4.9400(4) Å, b=8.5512(7) Å, c=5.0271(3) Å, β=109.28(6) °						
Atom	Wyckoff site	x	y	z	Occupancy	B_{iso} (Å^2)
Li	4h	0	0.306(3)	0.5	1	0.05
Mn	4g	0	0.169(4)	0	0.81	0.85(7)
Co	4g	0	0.169(4)	0	0.19	0.85(7)
Li	2a	0	0	0.5	1	0.05
Li	2b	0	0.5	0	0.61	0.1
Ni	2b	0	0.5	0	0.39	0.1
O	4i	0.269(3)	0	0.207(2)	1	0.97(25)
O	8j	0.249(2)	0.337(8)	0.228(9)	1	0.2 (1)

Table S2. Lattice parameters obtained from Le Bail fitting of the 1st sodiation and 101st sodiation samples.

O3a phase Space group: $R\bar{3}m$ a=b=2.9038(4) Å, c=16.3072(4) Å, α=β=90 °γ=120 °
O3b phase Space group: $R\bar{3}m$ a=b=2.8845(7) Å, c=15.1047(4) Å, α=β=90 °γ=120 °
O3a' phase Space group: $R\bar{3}m$ a=b=2.9153(2) Å, c=16.5635(15) Å, α=β=90 °γ=120 °
O3b' phase Space group: $R\bar{3}m$ a=b=2.8307(4) Å, c=15.0691(17) Å, α=β=90 °γ=120 °

Table S3. Detailed structural results obtained from fitting the ft-EXAFS Mn.

		Mn K-edge			
		Pristine	Fully sodiated	Ch3.0V	Ch3.8V
χ_r^2		21439.3223607	2734.10	2095.92	17575.6854917
S_0^2		0.59	0.59	0.59	0.59
CN	*O1*	6	6	6	6
	TM	2.6209±1.5468	4.267±1.437	4.497±1.609	4.8111±1.7019
Energy shift		-6.8526±2.4707	-2.847±1.814	-3.055±1.925	-7.538±1.891
σ^2*(* Å^2*)*	*O1*	0.00085±0.00129	0.00457±0.00123	0.00445±0.00132	0.00206±0.00124
	TM	-0.00185±0.00468	0.00324±0.00263	0.00372±0.00285	0.00301±0.00301
R (Å*)*	*O1*	1.89422±0.0160	1.88934±0.0131	1.88340±0.0140	1.88481±0.0132
	TM	2.86589±0.0202	2.88300±0.0132	2.86849±0.0145	2.87155±0.0157

Table S4. Detailed structural results obtained from fitting the ft-EXAFS Co.

		Co K-edge			
		Pristine	Fully sodiated	Ch3.0V	Ch3.8V
χ_r^2		1043.6314416	589.50	1844.66	1288.0459922
S_0^2		0.64	0.64	0.64	0.64
CN	6	6	6	6	6
	6	6	6	6	6
Energy shift		-4.715±1.545	-0.887±1.120	-0.781±1.831	-7.054±1.745
$\sigma^2(\text{Å}^2)$	*O1*	0.00125±0.00107	0.00337±0.00093	0.00337±0.00132	0.00147±0.00118
	TM	0.00419±0.00103	0.00435±0.00073	0.00429±0.00096	0.00318±0.00093
R (Å*)*	*O1*	1.91351±0.0119	1.90752±0.0099	1.90093±0.0145	1.89100 ±0.0125
	TM	2.85527±0.0126	2.85679±0.0092	2.84379±0.0133	2.84340 ±0.0125

Table S5. Detailed structural results obtained from fitting the ft-EXAFS Ni.

		Ni K-edge			
		Pristine	Fully sodiated	Ch3.0V	Ch3.8V
χ_r^2		10489.2875193	2145.55	1610.48	1242.7002371
S_0^2		0.81	0.81	0.81	0.81
CN	6	6	6	6	6
	6	6	6	6	6
Energy shift		-4.442±3.618	-1.204±2.333	-1.408±2.373	-2.258±5.137
σ^2(Å^2)	*O1*	0.00378±0.00656	0.0114±0.00278	0.0131±0.00305	0.0121±0.00298
	TM	0.00503±0.00255	0.00629±0.00105	0.00609±0.00111	0.00399±0.00179
R (Å)	*O1*	2.04614±0.0348	2.00232±0.0268	1.95562±0.0285	1.93662±0.0608
	TM	2.88712±0.0271	2.86784±0.00164	2.85190±0.0173	2.85739±0.0255

Reference

[1] A. P. Hammersley, S. O. Svensson, M. Hanfland, A. N. Fitch, D. Hausermann, *High Pressure Research* **1996**, *14*, 235-248.

[2] A. A. Coelho, *Journal of Applied Crystallography* **2018**, *51*, 210-218.

[3] X. Qiu, J. W. Thompson, S. J. L. Billinge, *Journal of Applied Crystallography* **2004**, *37*, 678-678.

[4] G. Hautier, S. P. Ong, A. Jain, C. J. Moore, G. Ceder, *Physical Review B* **2012**, *85*, 155208.

[5] a) S. Grimme, J. Antony, S. Ehrlich, H. Krieg, *The Journal of chemical physics* **2010**, *132*, 154104; b) S. Grimme, S. Ehrlich, L. Goerigk, *J. Comput. Chem.* **2011**, *32*, 1456-1465.

[6] J. L. Kaufman, J. Vinckevičiūtė, S. Krishna Kolli, J. Gabriel Goiri, A. Van der Ven, *Philosophical Transactions of the Royal Society A* **2019**, *377*, 20190020.

[7] a) Y. Idemoto, R. Kawai, N. Ishida, N. Kitamura, *Journal of Power Sources* **2015**, *273*, 1023-1029; b) D. Mohanty, A. Huq, E. A. Payzant, A. S. Sefat, J. Li, D. P. Abraham, D. L. Wood, C. Daniel, *Chemistry of Materials* **2013**, *25*, 4064-4070.

[8] A. Ito, Y. Sato, T. Sanada, M. Hatano, H. Horie, Y. Ohsawa, *Journal of Power Sources* **2011**, *196*, 6828-6834.

[9] a) J. Hu, B. Wu, X. Cao, Y. Bi, S. Chae, C. Niu, B. Xiao, J. Tao, J. Zhang, J. Xiao, *Journal of Power Sources* **2020**, *454*; b) Z. Shen, L. Cao, C. D. Rahn, C.-Y. Wang, *Journal of The Electrochemical Society* **2013**, *160*, A1842-A1846.